Highlights

High exposure of MoS_2 edges and d character of RuS_2 NPs

Very high hydrogen production rates **(10.2 l/h)**

Small Tafel slope and overpotential **(36 mV/decade, ~ 0.004 V)**

High performance as cathode in a PEM **(41.8 W power consumption)**

High hydrogen production rate on RuS_2@MoS_2 hybrid nanocatalyst by PEM electrolysis

Maria Sarno, Eleonora Ponticorvo

Department of Industrial Engineering and NANO_MATES Research Centre,

University of Salerno, via Giovanni Paolo II, 132 - 84084 Fisciano (SA), Italy

ABSTRACT

A new nanocatalyst, which combines the electrocatalytic activity of MoS_2 nanosheets and RuS_2 nanoparticles (NPs), was prepared through a safe and scalable, one-step "bottom-up" approach. It delivers high current density, with a Tafel slope of 36 mV/dec and a very small overpotential. The high exposure of MoS_2 edges on the RuS_2 NPs, the stronger *d* character of RuS_2 and the electrical coupling of these two nanomaterials, grown together, were responsible for the high hydrogen production rates of 10.2 l/h (PEM cell 5cm×5cm, current density about 1.1 A/cm^2, power consumption 41.8 W, corresponding to 3.8 KWh/Nm^3 of energy consumption, efficiency 93 %).

Keywords: RuS_2@MoS_2, high hydrogen production rate, PEM.

*Corresponding authors: Tel.: +39 089 963460; fax: +39 089 964057; E-mail address: msarno@unisa.it (M. Sarno).

Introduction

Among the different possibilities for hydrogen production, water electrolysis has numerous advantages, such as high purity, lack of pollution and it is a simple process. Hydrogen evolution reaction (HER) is faster in acidic environment rather than at other pHs [1]. However, because of corrosion issues, costly noble metals (Pt, Ir, Ru) are required [2]. Therefore, there is a major need for new active and cost-effective electrocatalysts for water splitting, which would offer low overpotential for hydrogen evolution in acidic media.

Ternary transition metal Chevrel-phase chalcogenides of Se and S are well known catalysts for industrial removal of oxygen, sulfur and nitrogen from refined petroleum products [3-6]. Chalcogenides of transition metals are a fascinating category of electrocatalysts, e.g. for ORR applications. MoS_2 nanostructures were successfully tested as catalysts for HER in acidic solution [7], showing how their electro-activity is dependent on the number of edge catalytic sites [8,9] and sulfur vacancies [10]. Numerous strategies have been developed to improve the electrocatalytic activity of MoS_2 [11]. However, most of these studies can only be proposed for laboratory applications and require complex procedures for its preparation. In any case, the main results exhibit a Volmer-Heyrovsky HER mechanism, with overpotential, exchange current density and tafel slope higher than 0.12 V, 0.2 mA/cm^2 and 44 mV/dec, respectively.

In fact, among different metal based chalcogenides, transition metals of group VIII show higher activity, e.g in the hydrodesulfuration (HDS) reaction [12]. In particular, the maximum activity is achieved by RuS_2 [13] because of its *d* orbitals electronic configuration. Indeed, RuS_2 *d* character, which is responsible for the surface coordinative unsaturation degree, is the highest [12,14]. Catalytic activity during HDS depends on the surface anion vacancies, allowing coordination with sulfur [13,15]. On the other hand, new active sites are generated by H_2, by removing sulfur from the surface and generating vacancies around the metals [16]. In particular, the interaction between hydrogen and catalyst surfaces most likely explains why an active catalyst for HDS is expected and still active for HER [10]. Ru–chalcogenides were tested as electrocatalyst materials [17], RuS_2 was

able to catalyze the oxygen reduction reaction (ORR) [18-21] and, because of its stability [22] even higher than that of MoS_2 [23], HER in hydrochloric or hydrobromic acids electrolyzes. Ruthenium based materials (Ru, RuO_2) have been widely used for various electrochemical applications, e.g. supercapacitors, sensors,..[24,25]. Although RuS_2 is a very stable and active material, it has never been tested for HER in H_2SO_4, nor in combination with MoS_2.

Proton exchange membrane (PEM) systems, which is the most promising technology for small scale production of H_2, have many advantages in comparison with traditional electrolyzers, e.g. pure water is the only reactant, very high purity products, lower costs for power and environmental impact, high specific productivity, direct production of high pressure gases and high degree of safety [26]. In PEM, due to the strong acidic conditions, platinum is typically used at the cathode to promote HER and iridium/iridium oxide at the anode to promote oxygen evolution reaction (OER). Different solutions have been proposed until now to reduce the cost of the electrode [27-29]. However, to the best of our knowledge, nanomaterials combining the promising properties of RuS_2 [30] and of MoS_2 nanosheets, have been never examined in PEM configuration. Our nanocatalyst enjoys the MoS_2 properties [9,31,32] amplified by the high edges exposure on the surface area of RuS_2 nanoparticles (NPs). In particular, in the nanocatalyst MoS_2 amount prevails on the more expensive RuS_2 [33], which is expected to be even more active. In this paper, we report the synthesis of a new nanocatalyst of MoS_2 and RuS_2 obtained through a one-step safe approach, from two solid phase precursors containing Ru, Mo and excess S. It shows very high exchange current density during hydrogen production, small Tafel slope and overpotential. The nanocatalysts were tested in a PEM configuration and for comparison in a flux of 0.5 M H_2SO_4 electrolyte, indeed measurements in 0.5 M H_2SO_4 simulate PEM environment, especially at the lower current density [34]. The continuous flow system was chosen to avoid bubble effects and better simulate a “real” electrolyzer.

Experimental

Samples synthesis

Ethanol (Fluka, 99.8%), hexane (Sigma-Aldrich, >95%), Benzyl ether (Aldrich, 99%), oleic acid (Aldrich, 90%), 1,2-hexadecanediol (Aldrich, 97%), oleylamine (Aldrich, 70%), ruthenium (III) acetylacetonate (Aldrich, 90%), ammonium tetrathiomolybdate (Aldrich, 99.97% metal basis) were acquired and used for the syntheses [35-37].

In particular: 0.6 mmol of ruthenium (III) acetylacetonate and 2.8 mmol of ammonium tetrathiomolybdate were dissolved in 18 mL of benzyl ether. Then, 8 mmol of 1,2-hexadecanediol, 4 mmol of oleylamine, 4 mmol of oleic acid were added. The solution was rapidly mixed and subjected to vigorous stirring to prevent formation of precipitates. The temperature was raised to 210 °C for 120 min and then to 285 °C for 120 min, under a nitrogen flow [7]. Ethanol (40 mL) was used for washing, followed by centrifugation. Finally, hexane was added (50 mL) and further centrifuged. The black/brown mixture was stored in a vial.

After synthesis, an annealing at 150 °C for 8 h was performed [7,37], preserving inorganic structure and morphology and improving electrical properties.

Characterization

SDTQ 600 (TA Instruments) Thermobalance (10 °C/min in air, equipped with a mass spectrometer; Bruker D8 X-ray diffractometer, Renishaw inVia Micro-Raman spectrometer (514 nm laser wavelength), PHI-550 Multitechnique X-ray photoelectron spectrometer, transmission electron microscopy (TEM) (FEI Tecnai electron microscope- 200 KV, coupled with an energy dispersive X-ray (EDX) probe) were used for characterization [7,37,38].

The electrochemical activity was evaluated by using the PGSTAT302N from Autolab potentiostat/galvanostat. For the measurements, SPEs (Dropsens (model 110), pseudo-reference electrode: Ag wire, counter and working electrodes: printed graphite were connected to the potentiostat. The whole apparatus comprises a peristaltic pump to feed a flow-through an amperometric cell, particularly designed to accommodate a SPE. Screen-printed electrodes are easy

to handle and facilitate the fast catalytic activity. The electrolyte flow wets perpendicular the SPE to obtain a wall-jet configuration [39]. Teflon with a good resistance in acid media was used for the electrochemical cell. A continuous flow of 0.5 M H_2SO_4 solution was provided by a peristaltic pump (DropSens Peristaltic Pump with 12 roller pump), polyethylene tubes were used for the electrolyte cycle from a vessel to the nanostructures. For the measurements, an ink was obtained mixing 4 mg of material with 80 μl of 5 wt% Nafion solution. For the test, the working electrodes were modified by dropping the nanostructures slurry/dispersion onto the surface.

Measurements have been also performed in a PEM configuration. In this case the whole apparatus (see Figure 1) comprises a peristaltic pump to feed to a splittable single unit flow cell at a flow rate of 40 ml min^{-1}. The PEM cell setup (5 cm×5 cm area) was equipped with a membrane (112 membrane - 51μm thick). The system has the potential to be vastly scaled up for industrial applications while incurring a lower cost increase, the capacity is scaled up by simply implementing a larger electrolyte tank. For the test, the membrane was modified by dropping the nanostructures slurry/dispersion onto one on the membrane surface (2 mg/cm^2), while the opposite face was modified by Ir (IV) oxide (IrO_2 >99 % , Alfa Aesar powder) with a fixed loading of 2 mg/cm^2 [40]. During HER the output gases were analyzed by a quadruple mass spectrometer (Thermo Scientific FOCUS GC-ISQ Single Quadrupole MS), while the chamber was flushed with nitrogen (10 Ncc/min) [7,41,42]. For H_2 evaluation, the areas of m/z = 2 MS was used, after a calibration curve evaluation [7,41,42].

Results and discussion

The morphological and structural characteristics of RuS_2@MoS_2 was determined by TEM analysis (Figure 2). In particular, the TEM images show nanoparticles with size in the range 8-10 nm. MoS_2 nanosheets, mostly monolayer, are clearly visible in Figure 2b and 2c, also MoS_2 edges laying on RuS_2 nanoparticles can be observed in these figures. The typical interplanar spacing of 0.279 nm for RuS_2 is revealed in Figure 2c. In the sample, free MoS_2 can be observed (Figure 2d), too. The

energy dispersive TEM based X-Ray spectroscopy (EDS) confirms the Ru/Mo ratio ~ 0.21 at., and sulfur S/(Ru+Mo) ratio ~ 2 .at.

XRD was conducted to obtain structural information of ruthenium and molybdenum sulfide. Figure 3 shows the XRD pattern of the synthesized product. The characteristic peaks shown in the pattern reveals the contemporaneous presence of RuS_2 and MoS_2. The main peaks coming from a cubic phase of RuS_2 (JCPDS 19-1107), can be observed. The broadening of diffraction peaks demonstrates that the size of the RuS_2 crystal is in a nanometer range. The typical peaks of MoS_2 obtained at a temperature lower than 360 °C, can be also seen. In particular, it is possible to assign the reflection peaks of the family lattices planes (100), (103), (104), (105), (110) and (112) of MoS_2 (JCPDS 17-0744).

Raman spectroscopy was used to analyze RuS_2@MoS_2 nanostructure (Figure 4). This is a very useful technique for the evaluation of the structure, bonding and degree of imperfections in nanostructures [43]. In general, the Raman spectrum of RuS_2 possesses E_g and A_g modes similar to those of MoS_2, ReS_2 and WS_2 [44,45]. The Raman spectrum in Figure 3 shows the presence of two bands at 376 and 387 cm^{-1} of the E_g and A_g modes of RuS_2, respectively. A shift of the sulfur atoms is responsible for the E_g mode, whereas the A_g mode corresponds to the stretching vibrational band of S-S [45,46]. Moreover, the E'_{2g} and A_{1g} modes for MoS_2 at about 382 and ~402 cm^{-1} [47] can be also seen. It has been found [48] that the difference between the positions of these two Raman modes is related to the number of MoS_2 layers. The frequency difference in cm^{-1} of the A_{1g} and E'_{2g} modes for MoS_2 indicate that most of the sheets have a number of layers between 1 and 2 [49].

In Figure 5, the X-ray photoelectron spectroscopy (XPS) analysis to evaluate the chemical states of the elements present in the RuS_2@MoS_2 nanoparticles is reported. The deconvolution of the spectrum in the range of Ru 3d evidence two peaks at 280.1 and 284.5 eV due to Ru $3d_{5/2}$ and Ru $3d_{3/2}$, respectively. Two peaks centered at 461.7 and 484.3 eV correspond to Ru $3p_{3/2}$ and Ru $3p_{5/2}$, respectively [50]. XPS spectrum in the region of Mo 3d shows two peaks at 229.1 and 232.3 eV, respectively, that can be attributed to Mo $3d_{5/2}$ and Mo $3d_{3/2}$. The peak at 226.6 eV can be indexed

as S 2s [51,52]. The deconvoluted spectrum of sulfur states highlighted the presence of four peaks centered at 162.1, 163.3, 162.4 and 163.9 eV corresponding to the S $2p_{3/2}$ and S $2p_{1/2}$ states for MoS_2, the first two, and RuS_2, the last two. From XPS analysis the atomic ratio between Ru and S results in 1:1.97, close to the stoichiometric of RuS_2, and it is 1:2.12 for MoS_2.

The thermogravimetric analysis of the RuS_2@MoS_2 is reported in Figure 6. During the thermal analysis of the nanostructures a decomposition/oxidation of the residual surfactants occurs together SO_2 formation [53]. At ~ 275 °C [53] the oxidation of MoS_2 to MoO_3 occurs, followed at about 528°C, by the decomposition/oxidation of RuS_2 [22]. The ratio of the weight losses between 275-528 °C and 528-925 °C, that are due to SO_2 release during contemporaneous formations of molybdenum and ruthenium oxide respectively, is equal to 0.217, in agreement with the ratio between the moles of ruthenium and molybdenum in the sample equal to 0.214.

Overall, the characterization confirms the successful preparation of a nanocatalyst consisting of RuS_2 nanoparticles covered by small edge size MoS_2 nanosheets.

Electrochemical hydrogen evolution reaction

Polarization curves for RuS_2@MoS_2 after IR-correction (i-V plot) are reported in Figure 7. RuS_2@MoS_2 activity for HER results excellent. A negligible overpotential (~ 0.004 V) and high rate of growth for cathodic current (840 mA/(V cm^2)) can be observed for RuS_2@MoS_2. Tafel equation ($\eta = b \log j + a$; η overpotential, b Tafel slope, j current density) was used to fit the linear region of the Tafel plot (Figure 8a). A Tafel slope of ~36 mV/decade and an exchange current density (j_0) of ~0.04 mA/cm^2 (iR-corrected) for RuS_2@MoS_2 were obtained, very close to the platinum behavior [54]. The observed Tafel slope for RuS_2@MoS_2 suggests that, on its surface, HER closely resembles the Volmer-Tafel mechanism [42,55-58], with the desorption step as the rate-limiting step.

It is worth noticing that MoS_2 typical Tafel slopes are in the range 50-80 mV/decade [11,35]. On the other hand, as far as RuS_2 is concerned, it has never been tested in H_2SO_4 electrolyte, while it

shows a Volmer-Heyrovsky mechanism in 0.5 HBr [23]. In particular, the sample after annealing shows a lower overpotential as a consequence of the reduced electrical resistance (Electrochemical impedance spectroscopy (EIS) evaluation, Figure 8b). The Nyquist plot indicated the presence of small semicircle at the high frequency region which arises due to the charge transfer resistance. The electrode exhibited small solution resistance (Rs) and charge transfer resistance (Rct) of about 0.35 and 1.9 V, respectively. The straight line or Warburg line (observed at low frequency region) is almost parallel to the imaginary axis which is related to the frequency dependent ion diffusion kinetics.

The synthesized RuS_2@MoS_2 was tested as cathode electrocatalyst in PEM. The performance of the RuS_2@MoS_2 was shown in comparison with commercial Pt/C catalyst in Figure 9. In particular, the behavior of 25 cm^2 PEM cell at 80 °C is reported. The performance of RuS_2@MoS_2 results quite close on that of Pt/C [40], indicating that the nanocatalyst not only behaves well at low current densities, where the behavior shown in 0.5 M H_2SO_4 and in PEM environment was found highly correlated [34] but continues to be efficient also when electrical/ionic resistivity and mass transport can affect significantly the electrocatalytic behavior.

Figure 10 shows the hydrogen production rate as a function of current obtained in the electrolyzer cell at a temperature of 80 °C. The production rate increases linearly with the increase of the current up to 10.2 l/h when the current intensity is about 1.1 A/cm^2, with a power consumption of 41.8 W, corresponding to 3.8 KWh/Nm^3 of energy consumption and an efficiency of 93 %.

The tests show for our nanocatalyst electrochemical performances extremely interesting, which were allowed thanks to the MoS_2 properties, amplified by the high edges exposure on the more active, because of its d band character, RuS_2 [33] NPs. In particular, they suggest that in the near future platinum could be replaced at the cathodes of PEM water electrolyzer.

Conclusions

An easy and safe approach has been chosen to produce RuS_2 nanoparticles covered by small edge size MoS_2 nanosheets. The nanoparticles of RuS_2 have a diameter of 8-10 nm and are mainly covered by one layer MoS_2. Additional, free MoS_2 is present in the sample, while the ratio between RuS_2 and MoS_2 results in agreement with the Ru, Mo molar ration in the precursor. The nanocatalyst exhibited a number of remarkable properties: Volmer-Tafel behavior, Tafel slope of 36 mV/dec and negligible overpotential, high exchange current density during hydrogen formation. The performance of the RuS_2@MoS_2 as cathode in a PEM evidence that the nanocatalyst not only behaves well at low energy densities but continues to be efficient also when electrical/ionic resistivity and mass transport can affect significantly the electrocatalytic activity.

References

[1] Danilovic N, Subbaraman R, Strmcnik D, Stamenkovic VR, Markovic NM. Electrocatalysis of the HER in acid and alkaline media. J Serb Chem Soc 2013;78:2007–15.

[2] Smiljanić M, Rakočević Z, Štrbac S, Electrocatalysis of hydrogen evolution reaction on tri-metallic Rh@Pd/Pt(poly) electrode. Int J Hydrogen Energy 2018;43:2763-71.

[3] Gullá AF, Gancs L, Allen RJ, Mukerjee S. Carbon-supported low-loading rhodium sulfide electrocatalysts for oxygen depolarized cathode applications. Appl Catal A Gen 2007;326:227–35.

[4] Alonso-Vante N. Carbonyl Tailored Electrocatalysts. Fuel Cells 2006;6:182–9.

[5] Babu PK, Lewera A, Chung JH, Hunger R, Jaegermann W, Alonso-Vante N, Wieckowski A, Oldfield E. Selenium Becomes Metallic in Ru−Se Fuel Cell Catalysts: An EC-NMR and XPS Investigation. J Am Chem Soc 2007;129:15140–1.

[6] Delacôte C, Lewer A, Pisarek M, Kulesza PJ, Zelenay P, Alonso-Vante N. The effect of diluting ruthenium by iron in Ru_xSe_y catalyst for oxygen reduction. Electrochim Acta 2010;55:7575–80.

[7] Sarno M, Ponticorvo E. Effect of the amount of nickel sulphide, molybdenum disulphide and carbon nanosupport on a Tafel slope and overpotential optimization. Nanotechnology 2017;28:214003–8pp.

[8] Jaramillo TF, Jørgensen KP, Bonde J, Nielsen JH, Horch S, Chorkendorff I. Identification of active edge sites for electrochemical H_2 evolution from MoS_2 nanocatalysts. Science 2007;317,100–2.

[9] Benson J, Li M, Wang S, Wang P, Papakonstantinou P. Electrocatalytic Hydrogen Evolution Reaction on Edges of a Few Layer Molybdenum Disulfide Nanodots. ACS Appl Mater Interfaces 2015;7:14113–22.

[10] Tsai C, Li H, Park S, Park J, Han HS, Nørskov JK, Zheng X, Abild-Pedersen F. Electrochemical generation of sulfur vacancies in the basal plane of MoS_2 for hydrogen evolution. Nat Commun 2017;8:15113.

[11] Miao J, Xiao F-X, Yang HB, Khoo SY, Chen J, Fan Z, Hsu Y-Y, Chen HM, Zhang H, Liu B. Hierarchical Ni-Mo-S nanosheets on carbon fiber cloth: A flexible electrode for efficient hydrogen generation in neutral electrolyte. Sci Adv 2015;1:1500259.

[12] Pecoraro TA, Chianelli RR. Hydrodesulfurization catalysis by transition metal sulfides. J Catal 1981;67:430–45.

[13] Aray Y, Rodríguez J, Vega D, Coll S, Rodríguez-Arias EN, Rosillo F. Adsorption of Thiophene on the RuS_2 (100) and (111) Surfaces: A Laplacian of the Electronic Charge Density Study. J Phys Chem B 2002;106:13242–9.

[14] Chianelli RR. Periodic Trends Transition Metal Sulfide Catalysis: Intuition and Theory. Oil Gas Sci Technol - Rev IFP 2006;61503–13.

[15] Hensen EJM, Brans HJA, Lardinois GMHJ, de Beer VHJ, van Veen JAR, van Santen RA. Periodic Trends in Hydrotreating Catalysis: Thiophene Hydrodesulfurization over Carbon-Supported 4d Transition Metal Sulfides. J Catal 2000;192:98–107.

[16] Rodriguez JA, Drovak J, Capitano AT, Gabelnick AM, Gland JL. Adsorption of thiophene on surfaces of clean and Ni-promoted molybdenum sulfide. Surf Sci 1999;429:L462–68.

[17] Alonso Vante N, Tributsch H. Energy conversion catalysis using semiconducting transition metal cluster compounds. Nature 1986;323:431–2.

[18] Zhang C, Yanagisawa K, Tao H, Onda A, Shou T, Kamiya S. Oxygen Reduction Activity and Methanol Resistance of Ru-based Catalysts Prepared by Solvothermal Reaction. Catal Lett 2012;142:1128–33.

[19] Solorza-Feria O, Ellmer K, Giersig M, Alonso-Vante N. Novel low-temperature synthesis of semiconducting transition metal chalcogenide electrocatalyst for multielectron charge transfer: molecular oxygen reduction. Electrochim Acta 1994;39:1647–53.

[20] Alonso-Vante N, Tributsch H, Solorza-Feria O. Kinetics studies of oxygen reduction in acid medium on novel semiconducting transition metal chalcogenides. Electrochim Acta 1995;40:567–76.

[21] Fischer C, Alonso-Vante N, Fiechter S, Tributsch H. Electrocatalytic properties of mixed transition metal tellurides (Chevrel-phases) for oxygen reduction. J Appl Electrochem 1995;25:1004–8.

[22] Li Y, Li N, Yanagisawa K, Li X, Yan X. Hydrothermal synthesis of highly crystalline RuS_2 nanoparticles as cathodic catalysts in the methanol fuel cell and hydrochloric acid electrolysis. Mater Res Bull 2015;65:110–5.

[23] Ivanovskaya A, Singh N, Liu R-F, Kreutzer H, Baltrusaitis J, Nguyen TV, Metiu H, McFarland E. Transition Metal Sulfide Hydrogen Evolution Catalysts for Hydrobromic Acid Electrolysis. Langmuir 2013;29:480–92.

[24] Krishnamoorthy K, Pazhamalai P, Kim SJ. Ruthenium sulfide nanoparticles as a new pseudocapacitive material for supercapacitor. Electrochim Acta 2017;227:85–94.

[25] Sarno M, Ponticorvo E, Scarpa D. Ru and Os based new electrode for electrochemical flow supercapacitors. Chem Eng J. *in press. https://doi.org/10.1016/j.cej.2018.09.211*

[26] Pakhomov VP, Fateev VN. Electrolysis of Water with Solid Polymer Electrolyte. Moscow, Russia: Preprint of Kurchatov Institute of Atomic Energy;1990.

[27] Carmo M, Fritz DL, Mergel J, Stolten D. A comprehensive review on PEM water electrolysis. Int J Hydrogen Energy 2013;38:4901–34.

[28] Grigoriev SA, Ilyukhina LI, Middleton PH, Millet P, Saetre TO, Fateev VN. A comparative evaluation of palladium and platinum nanoparticles as catalysts in PEM electrochemical cells. Int J of Nuclear Hydrogen Production and Applications 2008;1:343–54.

[29] Grigoriev SA, Porembsky VI, Fateev VN. Pure hydrogen production by PEM electrolysis for hydrogen energy. Int J Hydrogen Energy 2006;31:171-5.

[30] Mdleleni MM, Hyeon T, Suslick KS. Sonochemical Synthesis of Nanostructured Molybdenum Sulfide. J Am Chem Soc 1998;120:6189–90.

[31] Eftekhari A. Electrocatalysts for hydrogen evolution reaction. Int J Hydrogen Energy 2017;42:11053-77.

[32] Hai X, Zhou W, Wang S, Pang H, Chang K, Ichihara F, Ye J. Rational design of freestanding MoS_2 monolayers for hydrogen evolution reaction. Nano Energy 2017;39:409–17.

[33] Crum LA, Mason TJ, Reisse JL, Suslick KS, Eds. Sonochemistry and Sonoluminescence. Kluwer Academic Publishers: Dordrecht; 1999.

[34] Marshall A, Børresen B, Hagen G, Tsypkin M, Tunold R. Hydrogen production by advanced proton exchange membrane (PEM) water electrolysers—Reduced energy consumption by improved electrocatalysis. Energy 2007;32:431–6.

[35] Sarno M, Cirillo C, Garamella A, Ciambelli P. Synthesis and Characterization of Electrocatalytic graphene/MoS_2/Ni Nanocomposites. Chem Eng Trans 2014;41:217–22.

[36] Altavilla C, Sarno M, Ciambelli P. Synthesis of Ordered Layers of Monodisperse $CoFe_2O_4$ Nanoparticles for Catalyzed Growth of Carbon Nanotubes on Silicon Substrate. Chem Mater 2009;21:4851–8.

[37] Sarno M, Ponticorvo E, Cirillo C. High surface area monodispersed Fe_3O_4 nanoparticles alone and on physical exfoliated graphite for improved supercapacitors. J Phys Chem Solids 2016;99:138–47.

[38] Ferrara M, Neitzert H-C, Sarno M, Gorrasi G, Sannino D, Vittoria V, Ciambelli P. Influence of the electrical field applied during thermal cycling on the conductivity of LLDPE/CNT composites. Physica E Low Dimens Syst Nanostruct 2007;37:66-71.

[39] Yamada J, Matsuda H. Limiting diffusion currents in hydrodynamic voltammetry: III. Wall jet electrodes. J Electroanal Chem Interfacial Electrochem 1973;44:189–98.

[40] Marshall AT, Sunde S, Tsypkin M, Tunold R. Performance of a PEM water electrolysis cell using $Ir_xRu_yTa_zO_2$ electrocatalysts for the oxygen evolution electrode. Int J Hydrogen Energy 2007;32:2320–4.

[41] Sarno M, Ponticorvo E. Much enhanced electrocatalysis of Pt/PtO_2 and low platinum loading Pt/PtO_2-Fe_3O_4 dumbbell nanoparticles. Int J Hydrogen Energy 2017;42:23631–8.

[42] Sarno M, Ponticorvo E. Continuous flow HER and MOR evaluation of a new Pt/Pd/Co nano electrocatalyst. Appl Surf Sci 2018;459:105–13.

[43] Deokar G, Vignaud D, Arenal R, Louette P, Colomer J-F. Synthesis and characterization of MoS_2 nanosheets. Nanotechnology 2016;27:075604–10pp.

[44] Thripuranthaka M, Kashid RV, Rout CS, Late DJ. Temperature dependent Raman spectroscopy of chemically derived few layer MoS_2 and WS_2 nanosheets. Appl Phys Lett 2014;104:081911-5.

[45] Taguchi I, Vaterlaus HP, Bichsel R, Levy F, Berger H, Yumoto M. Raman scattering study of phonons in RuS_2 and $RuSe_2$ single crystals. J Phys C: Solid State Phys 1987;20:4241–50.

[46] Lin SS, Huang YS, Huang CR, Lee MC. Raman investigation of RuS_2. Solid State Commun 1989;69:589–93.

[47] Altavilla C, Sarno M, Ciambelli P, Senatore A, Petrone V. New 'chimie douce' approach to the synthesis of hybrid nanosheets of MoS_2 on CNT and their anti-friction and anti-wear properties. Nanotechnology 2013;24:125601–11pp.

[48] Lee C, Yan H, Brus LE, Heinz TF, Hone J, Ryu S. Anomalous Lattice Vibrations of Single- and Few-Layer MoS_2. ACS Nano 2010;4:2695–700.

[49] Sarno M, Garamella A, Cirillo C, Ciambelli P. MoS_2 Nanosheets for HER and LIB. Chem Eng Trans 2014;41:391–6.

[50] Jaegermann W, Kühne H-M. XPS analysis of the oxidation reaction of ruthenium-chalcogenide photoelectrodes. Appl Surf Sci 1986;26:l–11.

[51] Wang HW, Skeldon P, Thompson GE, Wood GC. Synthesis of molybdenum disulphide by acidification of ammonium tetrathiomolybdate solutions. J Mater Sci Lett 1996;15:494–6.

[52] Wang, HW, Skeldon, P; Thompson, G. E. XPS studies of MoS_2 formation from ammonium tetrathiomolybdate solutions. Surf Coat Technol 1997;91:200–7.

[53] Sarno M, Troisi A. Supercapacitors Based on High Surface Area MoS_2 and MoS_2–Fe_3O_4 Nanostructures Supported on Physical Exfoliated Graphite. J Nanosci Nanotechnol 2017;17:3735–43.

[54] Han X, Tong X, Liu X, Chen A, Wen X, Yang N, Guo X-Y. Hydrogen Evolution Reaction on Hybrid Catalysts of Vertical MoS_2 Nanosheets and Hydrogenated Graphene. ACS Catal 2018;8:1828–36.

[55] Hinnemann B, Moses PG, Bonde J, Jørgensen KP, Nielsen JH, Horch S, Chorkendorff I, Nørskov JK. Biomimetic Hydrogen Evolution: MoS_2 Nanoparticles as Catalyst for Hydrogen Evolution. J Am Chem Soc 2005;127:5308-9.

[56] Ma T, Zhang M, Liu H, Wang Y, Pan D. Synthesis of novel three-dimensional mesoporous nitrogen doped graphene supported Pt nanoparticles as superior catalyst for hydrogen generation. Int J Hydrogen Energy 2018;43:19327-35.

[57] Zhang Y, Zang J, Han C, Jia S, Tian P, Gao H, Wang Y. Molybdenum oxide and molybdenum carbide coated carbon black as an electrocatalyst for hydrogen evolution reaction in acidic media. Int J Hydrogen Energy 2017;42: 26985-94.

[58] Li Y, Wang H, Xie L, Liang Y, Hong G, Dai H. MoS_2 Nanoparticles Grown on Graphene: An Advanced Catalyst for the Hydrogen Evolution Reaction. J Am Chem Soc 2011;133:7296-9.

Figure

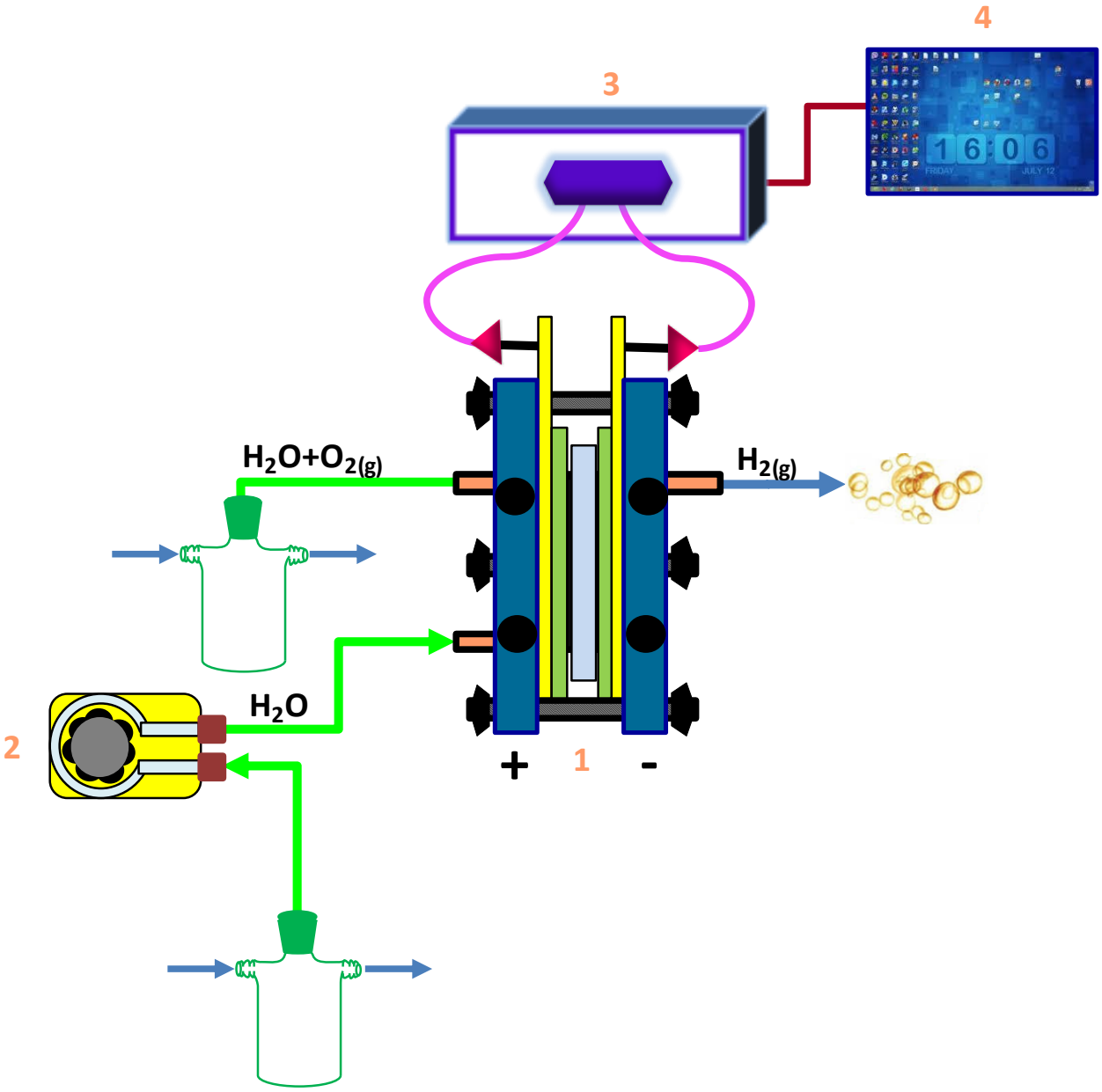

Figure 1 PEM Electrolyser system: (1) electrochemical reaction cell, (2) peristaltic pump and water reservoir, (3) potentiostat/galvanostat and (4) computer.

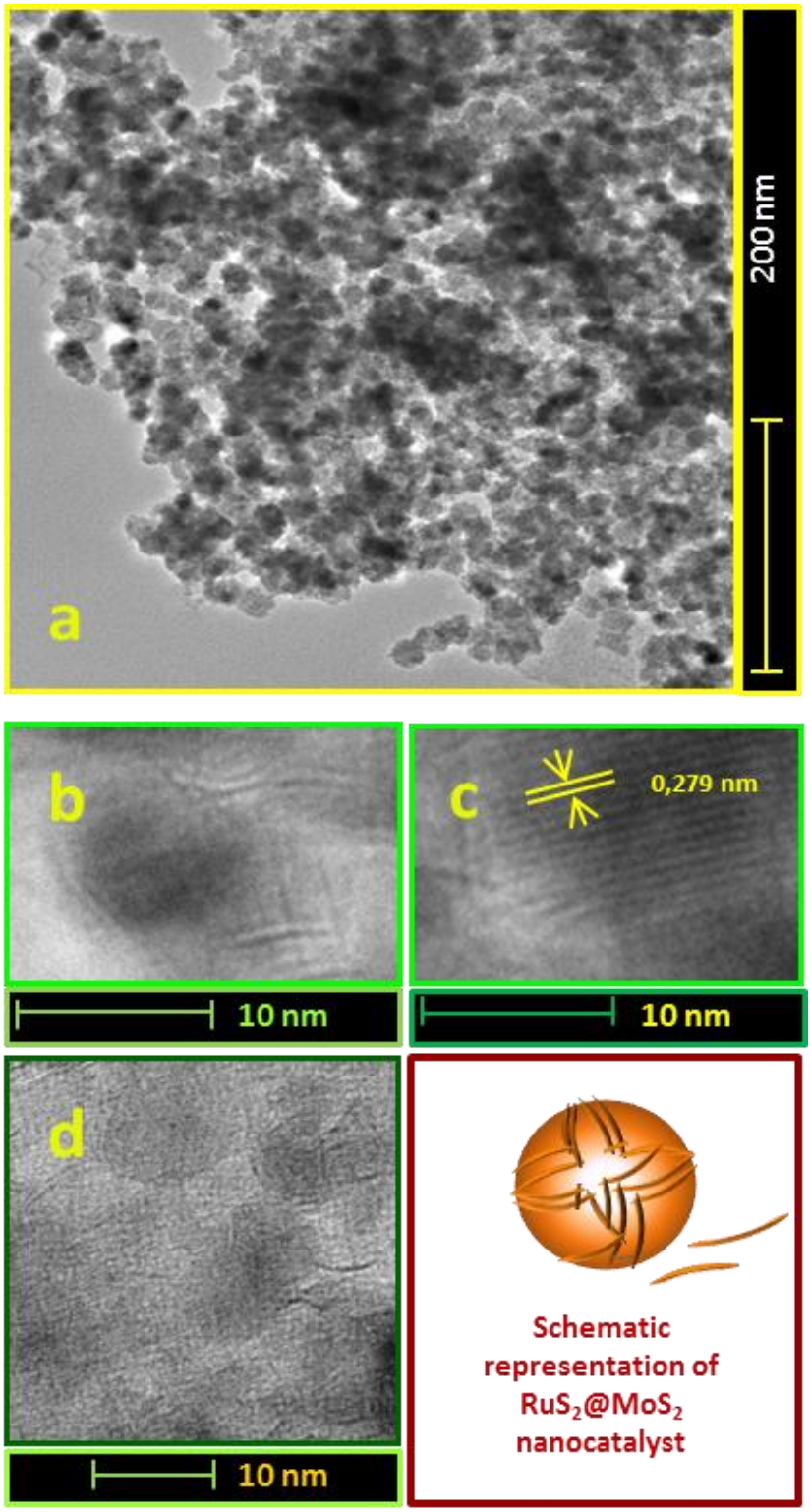

Figure 2 TEM images of RuS_2@MoS_2 nanocatalyst at lower (a) and higher magnifications (b,c,d). Schematic representation at the bottom.

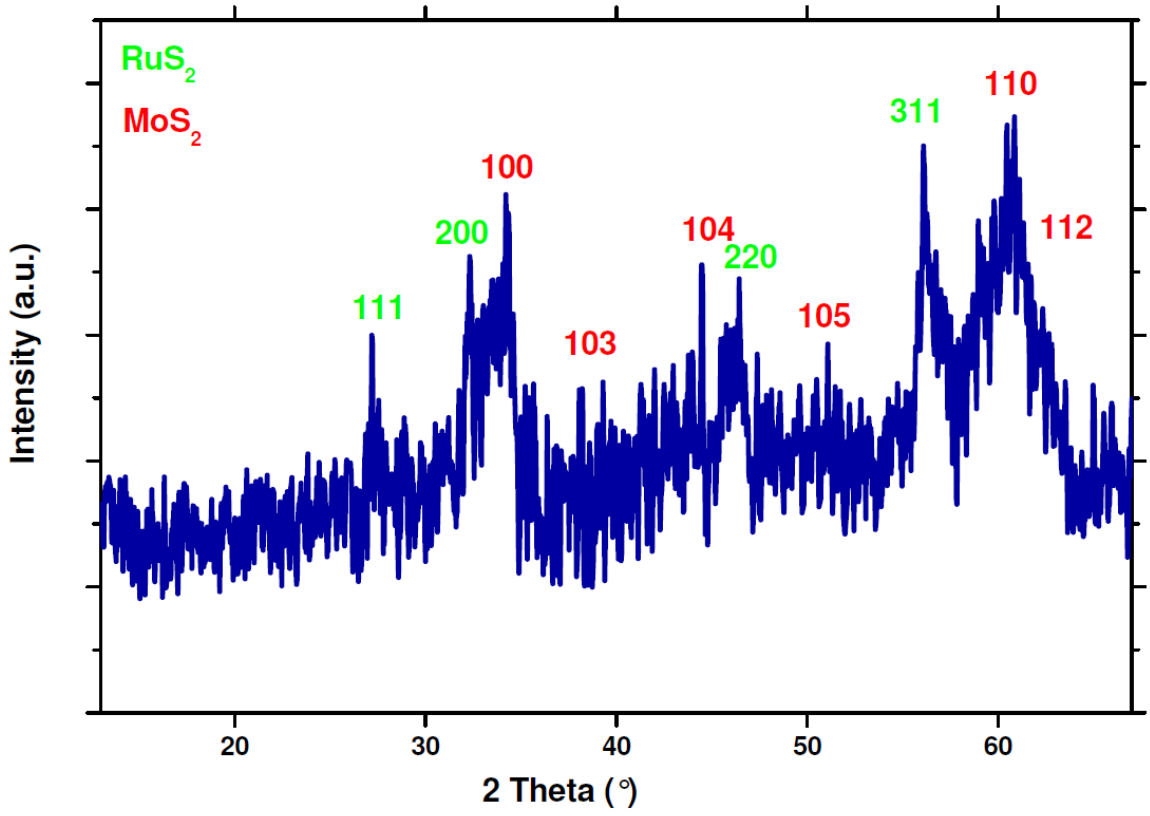

Figure 3 XRD diffraction pattern of RuS_2@MoS_2 nanocomposite.

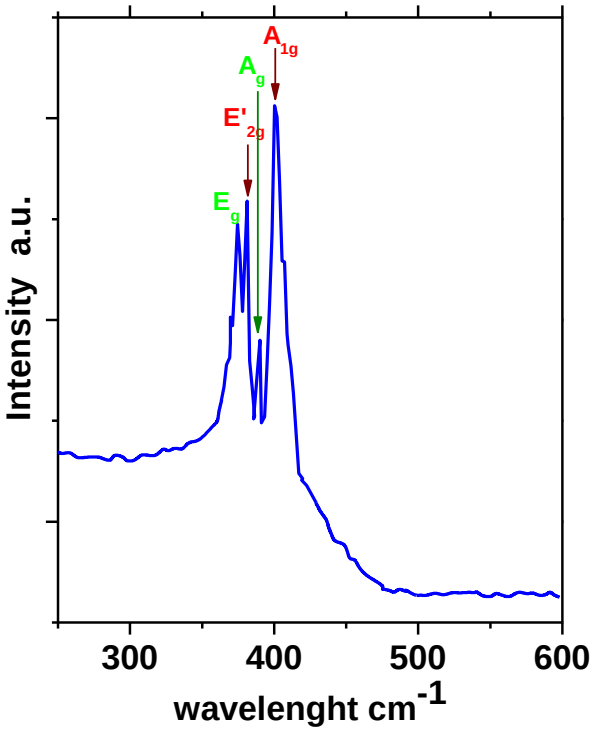

Figure 4 Raman spectrum of RuS_2@MoS_2 nanocomposite.

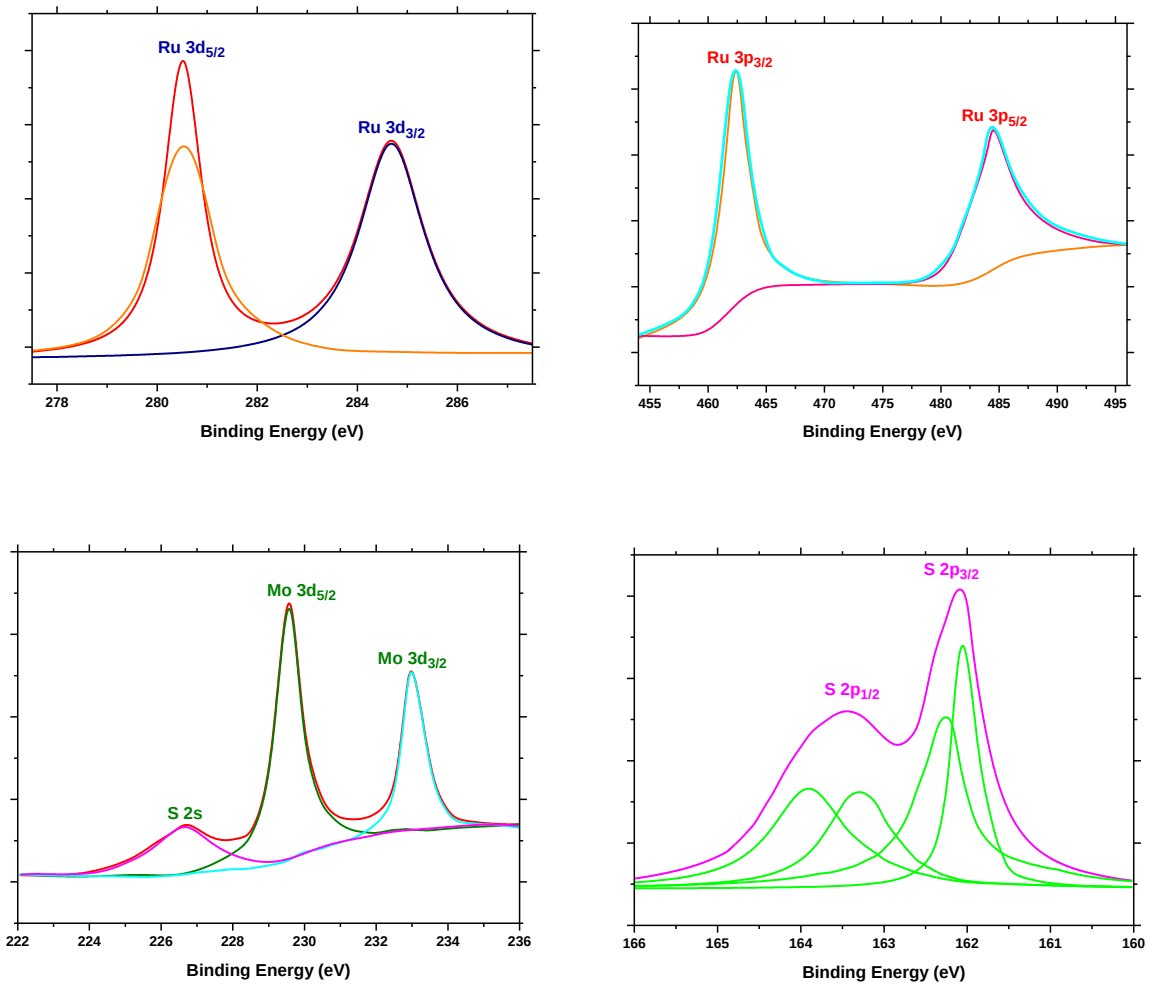

Figure 5 XPS spectra of RuS_2@MoS_2 in the Ru 3d, Ru 3p, Mo 3d and S 2p regions.

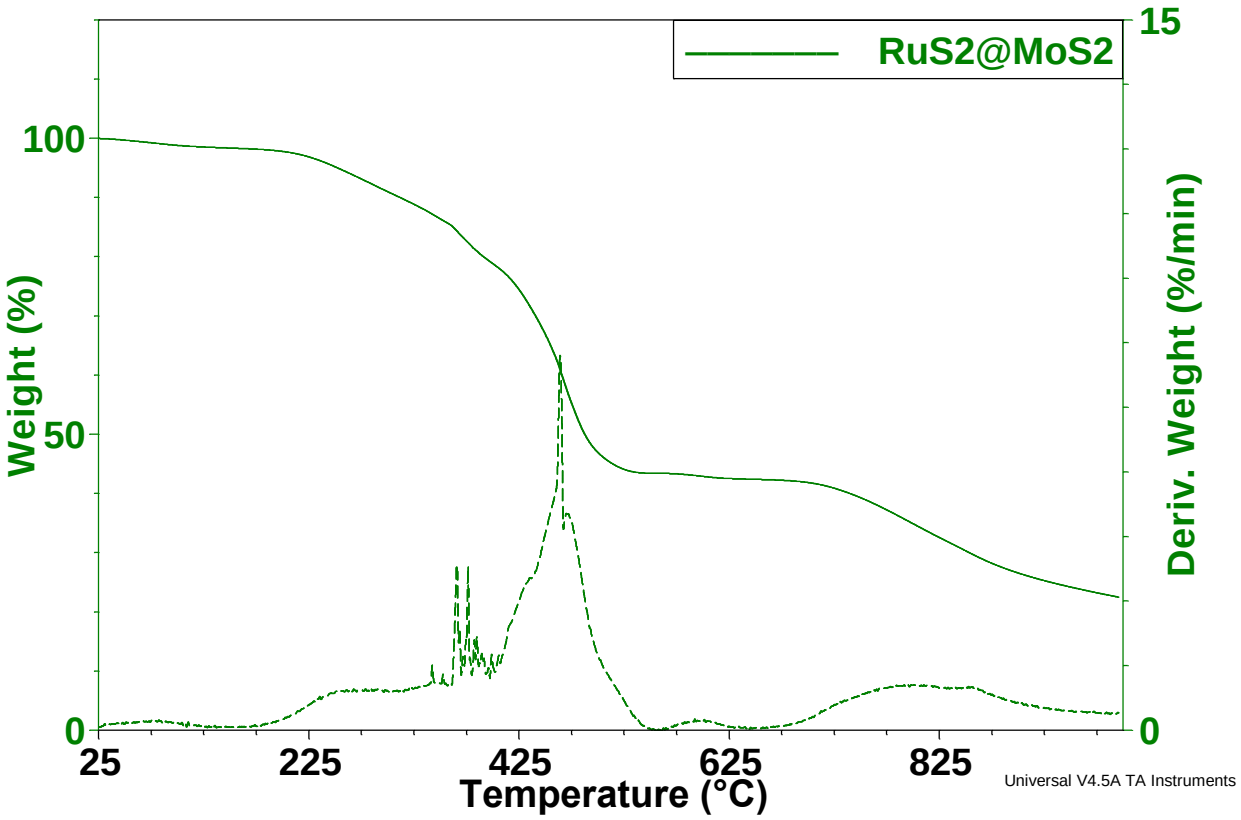

Figure 6 TG-DTG analysis of the RuS_2@MoS_2.

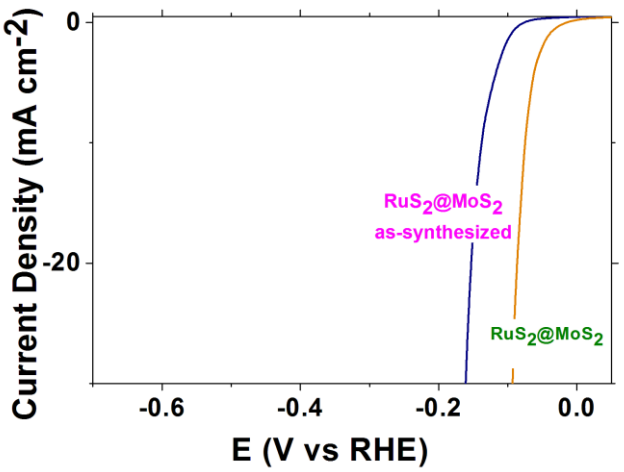

Figure 7 Polarization curves at 20 mV/sec of $RuS_2@MoS_2$ nanocomposite.

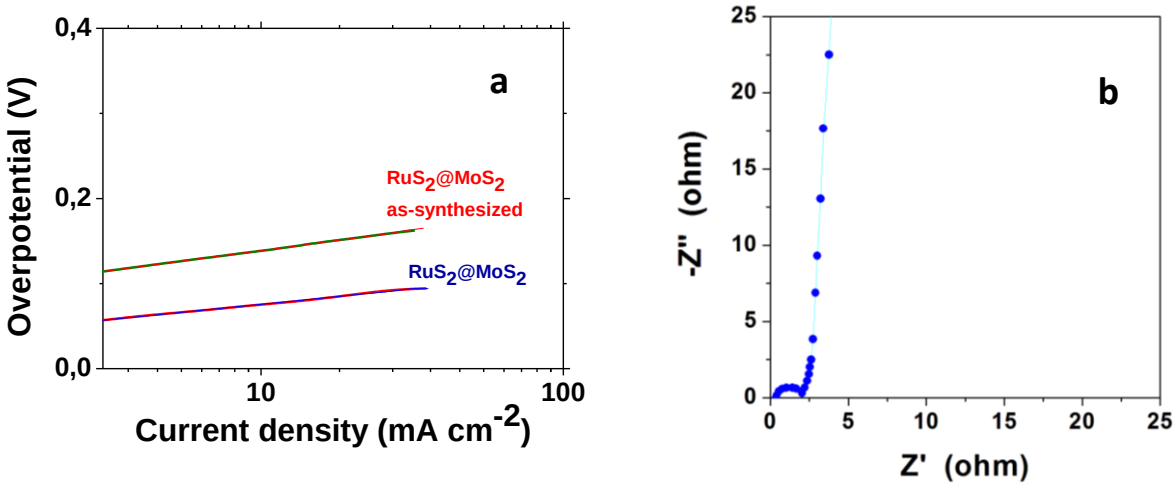

Figure 8 Tafel plot (a) and EIS analysis (b) for $RuS_2@MoS_2$.

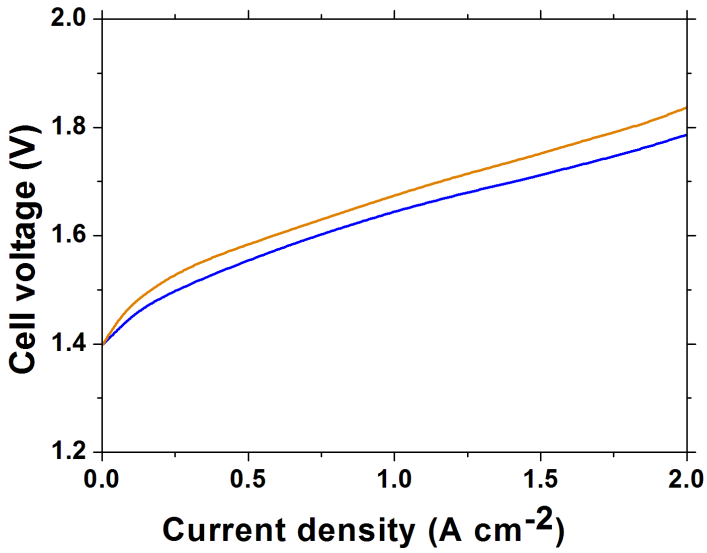

Figure 9 Polarization curve for PEM water electrolyzer of Pt in blue and RuS_2@MoS_2 in orange at 80°C.

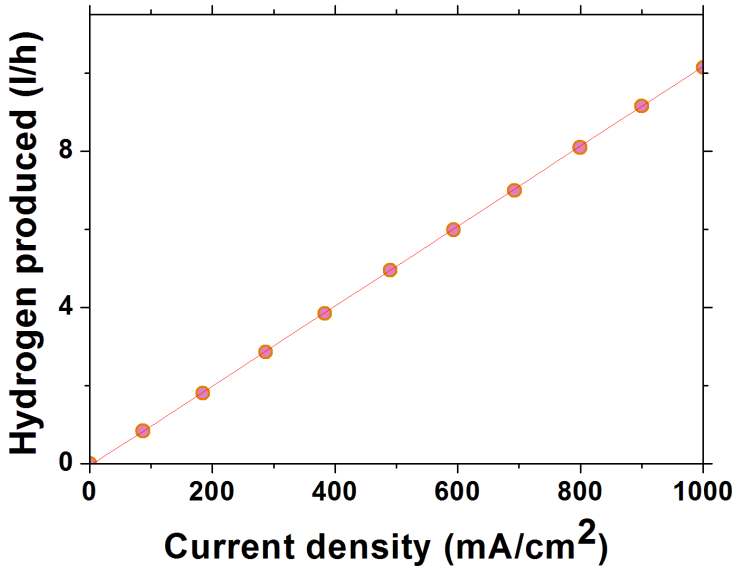

Figure 10 Hydrogen production rate for RuS_2@MoS_2 PEM water electrolyzer with operation current density.